Geochemistry Geophysics Geosystems G3

Article
Volume 13, Number 1
11 February 2012
Q02005, doi:10.1029/2011GC004009
ISSN: 1525-2027

Published by AGU and the Geochemical Society

Analysis of 60 elements in 616 ocean floor basaltic glasses

Frances E. Jenner
Research School of Earth Sciences, Australian National University, Canberra, ACT 0200, Australia

Department of Terrestrial Magnetism, Carnegie Institution of Washington, 5241 Broad Branch Road Northwest, Washington, DC 20015, USA (fjenner@dtm.ciw.edu)

Hugh St. C. O'Neill
Research School of Earth Sciences, Australian National University, Canberra, ACT 0200, Australia

[1] The abundances of 60 elements in 616 Ocean Floor Basaltic (OFB) glasses from the Abyssal Volcanic Glass Data File (AVGDF) of the Smithsonian Institution have been determined by laser-ablation (LA)-ICP-MS and electron microprobe analysis (EMPA). The elements analyzed include all 28 of the refractory lithophile elements, which provide the framework for establishing the geochemical behavior and source abundances of volatile, chalcophile and siderophile elements. In addition to the traditionally analyzed elements (rare earth elements (REE), high field strength elements (HFSE), large ion lithophile elements (LILE) and first row transition elements (FRTE)), we report analyses for lesser-analyzed elements (Li, Be, Ga, Ge, As, Se, Mo, Ag, Cd, In, Sn, Sb, W, Tl and Bi). The precision of the method for most elements is between 2 and 4%, one standard deviation, although ratios of elements determined simultaneously are more precise (e.g., REE, Zr/Hf). Subsets of 329 glasses were analyzed by electron microprobe for S and 154 glasses for Cl. The results define a representative trace element geochemistry of OFB, against which local variations resulting from differences in basalt petrogenesis in a range of tectonic settings or different styles of magmatic differentiation may be compared.

Components: 4600 words, 8 figures.

Keywords: LA-ICP-MS; MORB; data file; geochemistry; ocean floor basalt; volcanic glass.

Index Terms: 1032 Geochemistry: Mid-oceanic ridge processes (3614, 8416); 1065 Geochemistry: Major and trace element geochemistry; 3614 Mineralogy and Petrology: Mid-oceanic ridge processes (1032, 8416).

Received 16 December 2011; **Accepted** 5 January 2012; **Published** 11 February 2012.

Jenner, F. E., and H. St. C. O'Neill (2012), Analysis of 60 elements in 616 ocean floor basaltic glasses, *Geochem. Geophys. Geosyst.*, *13*, Q02005, doi:10.1029/2011GC004009.

1. Introduction

[2] Basaltic magmatism associated with rifting in ocean basins, such as at mid-ocean ridges and associated fracture zones and seamounts, comprises about 75% of all magmatism on Earth [e.g., *Crisp*, 1984], with a flux averaged over the last 180 Ma of ~20 km^3 per annum [*Cogné and Humler*, 2006]. The most accessible parts of the magmatic output are the lavas erupted onto the ocean floor, where rapid quenching of lava flow surfaces by seawater forms volcanic glass. Volcanic glasses are attractive analytical targets because they sample the magmatic liquid compositions directly, whereas

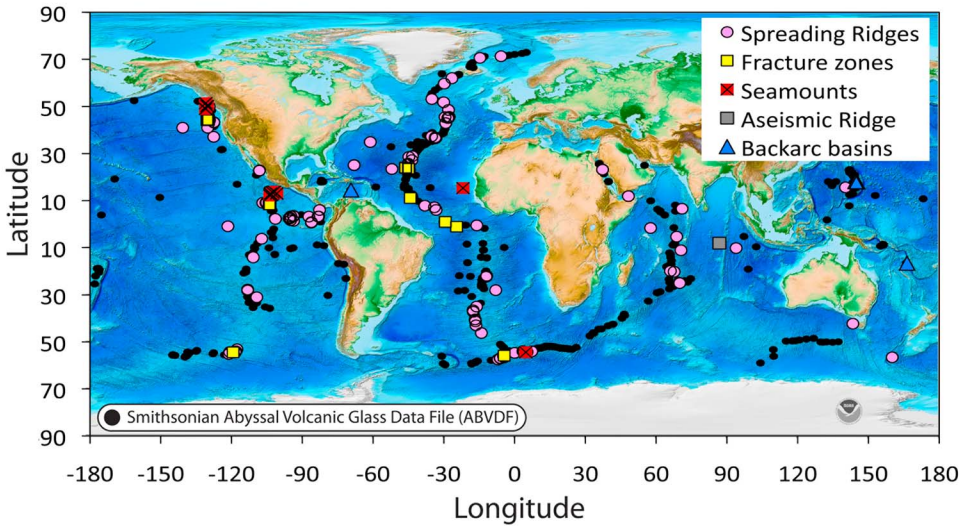

Figure 1. Locations of samples in the Smithsonian Abyssal Volcanic Glass Data File (AVGDF; black symbols) and those analyzed for this study. Base map from *Amante and Eakins* [2009].

crystalline basalts are mixtures of the evolved liquid with phenocrysts, which may not all be cognate with the liquid. Crystalline basalts are prone to contamination by low temperature alteration, which may be difficult to detect a priori. Elements concentrated in phases highly susceptible to alteration, such as sulfides, may be particularly affected [e.g., *Keays*, 1987]. Additionally, rapidly quenched volcanic glasses are likely to retain volatiles better than crystallized rock. While typical MORB glasses have degassed some CO_2 [e.g., *Aubaud et al.*, 2004; *Paonita and Martelli*, 2007], their retention of other volatiles like H_2O and S is better than that in crystallized rock, which should minimize any loss of volatile trace elements.

[3] The Smithsonian Institution has been donated thousands of volcanic glass samples, retrieved by dredging and coring of the ocean floor (black symbols in Figure 1). These glasses have been mounted in epoxy and polished for analysis of major elements by electron microprobe (EMPA), with results collated into the Abyssal Volcanic Glass Data File (AVGDF) [*Melson et al.*, 2002, 1976]. The last published version of this file [*Melson et al.*, 2002] contains 9050 analyses, from 664 Atlantic, 28 Caribbean, 89 Indian, and 1304 Pacific localities. LA-ICP-MS provides the opportunity for obtaining precise trace element analyses of samples in the AVGDF. Nearly all the trace elements can be determined by this method, including the rare earth elements (REE), high field strength elements (HFSE), large ion lithophile elements (LILE), first row transition elements (FRTE), as well as the less commonly analyzed elements such as Li, Be, Cu, Zn, Ga, Ge, As, Se, Mo, Ag, Cd, In, Sn, Sb, W, Tl and Bi with a precision that can be demonstrated by replication to be 1–3% [e.g., *Hu et al.*, 2009; *Jochum et al.*, 2006; *Jenner and O'Neill*, 2012].

[4] Here we report the results of LA-ICP-MS analyses of ~60 elements in 616 OFB glasses, kindly made available to the authors by the Smithsonian Institution [see *Melson et al.*, 2002]. Our aim is to generate a reference data set for trace element geochemistry of OFB, against which the compositions of basalts from specific localities or from other tectonic environments may be compared. A feature of this study is the large number of elements analyzed on individual samples, which enables the comparative chemistry of the less familiar trace elements to be established. By analyzing all the 28 refractory lithophile elements (RLE; Ca, Al, REE, Ti, Be, Ba, Sc, Sr, Y, Zr, Nb, Hf, Ta, Th and U), we provide the complete framework needed to estimate the Bulk Silicate Earth (BSE) abundances of those volatile, chalcophile and siderophile elements that are obtained from ratios with a RLE of similar incompatibility during magmatic processes [e.g., *Palme and O'Neill*, 2003]. The behavior of chalcophile elements like Cu, Se and Ag is controlled by sulfide saturation, the better understanding of which requires knowledge of S contents, which we have measured in 329 glasses by EMPA. Another subset of 154 glasses were analyzed for Cl by EMPA, because high Cl could be a potential indicator of

seawater contamination. We also include approximate contents for Re, Pt and Au in a subset of samples (previously published in the study by *Jenner et al.* [2010]).

2. Analytical Methods

[5] A full description of the trace element analyses by laser-ablation ICP-MS is given in the study by *Jenner and O'Neill* [2012]. Sample preparation and details of the major element analyses by EMPA used to generate the AVGDF are given by *Melson et al.* [2002]. EMPA analysis was used on 329 of the samples for S contents and 154 for Cl on the Cameca SX100 electron microprobe at the Research School of Earth Sciences (RSES). Because the position of the sulfur K-alpha peak shifts as a function of valence state, sulfur calibrations and analyses of unknowns were carried out by scanning over the entire sulfur peak and background on either side, in 200 steps, using PET crystals in one or two spectrometers with a counting time of 500 s. Analyses were undertaken with a defocused beam of 20 μm diameter, at an accelerating voltage of 15 kV and 100 nA beam current. Calibration used both sulfide (troilite; FeS) and sulfate (anhydrite; $CaSO_4$) standards, which gave identical results. For some samples, one of the spectrometers with a PET crystal was used to analyze Cl, with scapolite (1.43% Cl) as the standard. Reported values are the mean and standard deviation of at least five replicate analyses on each sample. Typical limits of detection for S and Cl on each analysis are $\sim$50 $\mu g\ g^{-1}$.

[6] VG-2 [*Jarosewich et al.*, 1979], was analyzed during each analytical session to monitor instrument performance (Table S1 in the auxiliary material).[1] The mean abundance, standard deviation (s) and standard error of the mean (s.e.; calculated as $s/n^{1/2}$), for S (n = 247) and Cl (n = 119) analyzed in VG-2 over the length of this analytical project ($\sim$2 years) are 1415 $\pm$ 68 $\mu g\ g^{-1}$ (s.e. = 4) and 301 $\pm$ 24 $\mu g\ g^{-1}$ (s.e. = 2), respectively. The Cl contents measured in VG-2 are within error of previous measurements, for example: 300 $\mu g\ g^{-1}$ [*Jarosewich et al.*, 1979]; 303 $\pm$ 56 $\mu g\ g^{-1}$ [*de Hoog et al.*, 2001]; 296 $\pm$ 19 $\mu g\ g^{-1}$ [*Laubier et al.*, 2007]; 290 $\pm$ 35 $\mu g\ g^{-1}$ [*Kamenetsky et al.*, 2007]; and 272 $\pm$ 83 $\mu g\ g^{-1}$ [*Baker*, 2008]. Literature values for S were reviewed by *O'Neill and Mavrogenes* [2002], who themselves reported 1403 $\pm$ 31 $\mu g\ g^{-1}$. Additional studies not listed by *O'Neill and Mavrogenes* [2002] are: 1400 $\pm$ 115 $\mu g\ g^{-1}$ [*Kamenetsky et al.*, 2007]; 1405 $\pm$ 39 $\mu g\ g^{-1}$ [*Baker*, 2008]; 1362 $\pm$ 160 $\mu g\ g^{-1}$ [*Davis et al.*, 2008].

[7] Analyses of S in OFB that showed higher than 10% relative standard deviation (RSD) were reanalyzed at a later date to test whether the scatter reflected real heterogeneity in the sample or analytical problems. This confirmed that 17 of the OFB show significant variability in S contents (RSD between 10 and 17%). This heterogeneity may indicate some partial loss of S by degassing, or localized scavenging into immiscible sulfide globules [*Peach et al.*, 1990], which are likely present in nearly all MORB melts, because they are at or near sulfide saturation [*Mathez*, 1976]. Nevertheless, the average RSD for all samples is 4.7%, demonstrating that such effects are rare. Of the Cl analyses, 47 glasses contained Cl below the limit of detection. For the samples where Cl was quantifiable, there is an increase to higher RSD with decreasing Cl content as the Cl content approaches the limit of detection. The average RSD for all samples is 7.5%. Hence, the determination of Cl in OFB glasses would benefit from a more sensitive technique like SIMS, with detection limits of $< 1\ \mu g\ g^{-1}$ for Cl [e.g., *Hauri et al.*, 2002].

[8] The analytical results are presented in Table S2, compiled with major element analyses from *Melson et al.* [2002]. Major elements analyzed by LA-ICP-MS show good agreement with the EMPA data, except for Ca and Fe in 31 samples (sample numbers shown in Table S2), for which the AVGDF analyses were found to be wrong, possibly resulting from a mix up of the computer punch cards (T. O'Hearn, personal communication, 2007). Consequently, we substitute our EMPA values of Ca and Fe for these samples.

3. Discussion

3.1. Geographic and Geochemical Sampling of the AVGDF

[9] The samples analyzed are from the Atlantic (n = 307), Pacific (n = 265), Indian (n = 41) and the Caribbean Ocean (n = 3), and represent most of the major geographical regions, with their varying spreading rates and local tectonic environments (Figures 1 and 2). Only a few samples were available from the Southwest and Southeast Indian Ridges and the Pacific-Antarctic Ridge (Figure 1). The distribution in MgO of samples analyzed for

[1] Auxiliary materials are available in the HTML. doi:10.1029/2011GC004009.

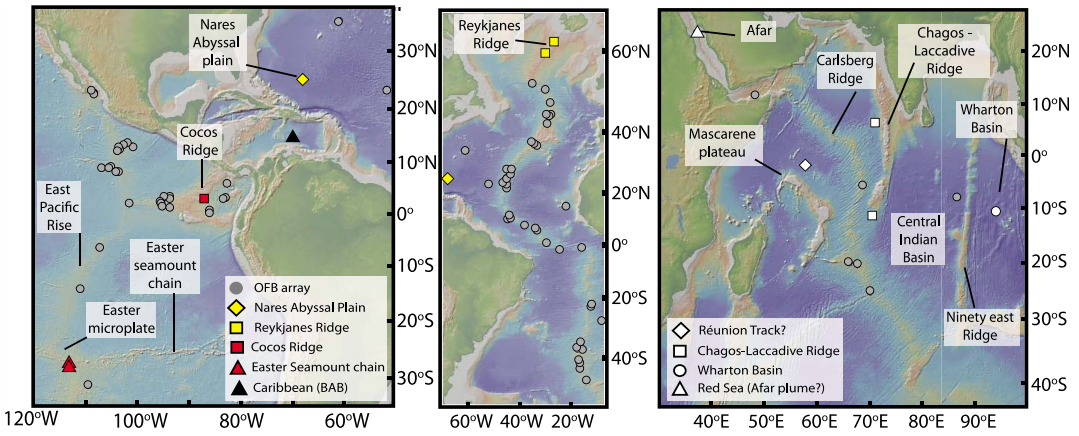

Figure 2. Seafloor maps generated using GeoMapApp (http://www.geomapapp.org) with base map from *Ryan et al.* [2009], demonstrating that some of the samples designated as 'spreading ridges' in the AVGDF occur along ridges associated with proposed plume tracks. Colored symbols show locations of samples with higher Cu at a given MgO (Figure 3d) than the majority of the OFB array (gray symbols).

this study (Figure 3) demonstrates that the range in analyses are approximately representative of the entire AVGDF, except for a slight bias to more primitive compositions, because we analyzed all samples made available to us with MgO > 8 wt.%. The samples cover a range in major element chemistries from primitive to moderately evolved (9.7 to ~ 3.5 wt.% MgO) (Figure 3). The distributions of P, K and Ti of the analyzed samples are comparable to those of the entire AVGDF (Figure 4), in which

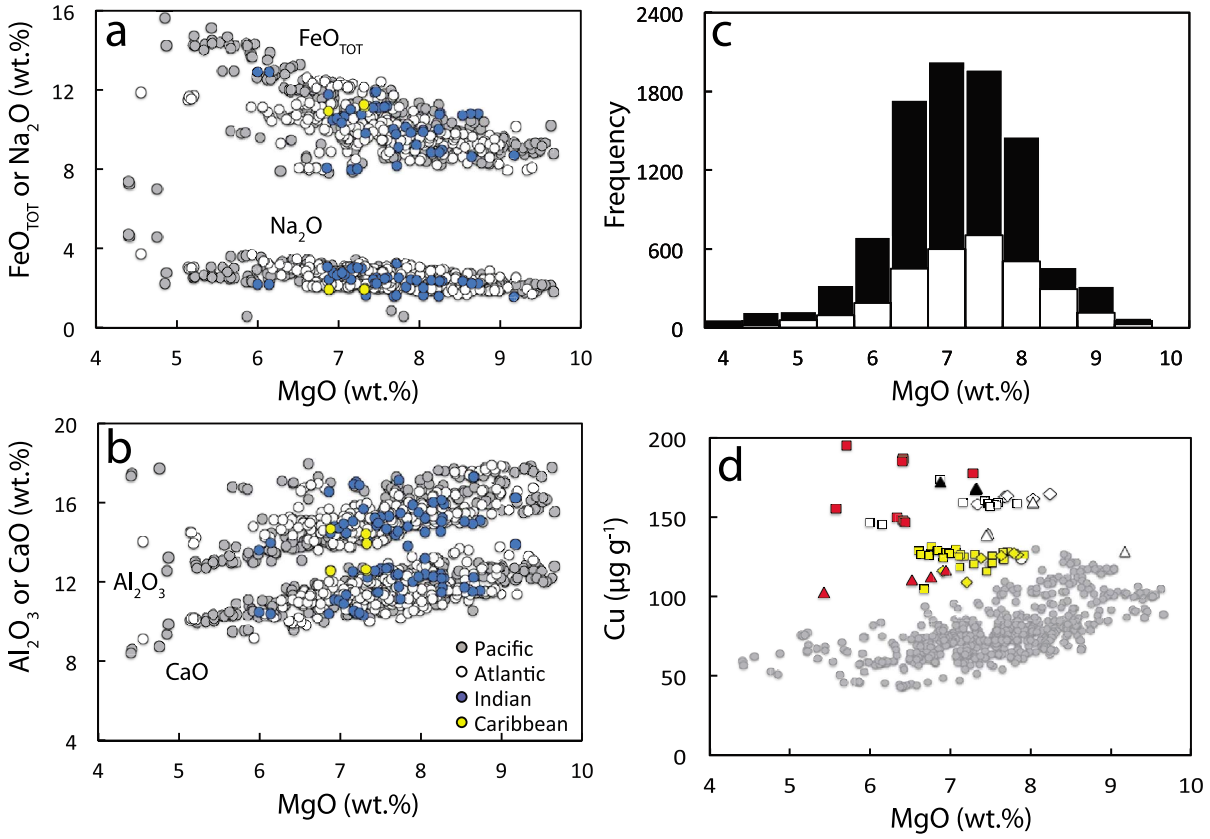

Figure 3. (a, b) Major oxide versus MgO of analyzed samples. (c) The distribution of MgO in the analyzed samples compared to the whole AVGDF. (d) Samples from a number of localities that may be plume-related (symbols same as Figure 2) show higher Cu contents at a given MgO than the majority of the OFB array.

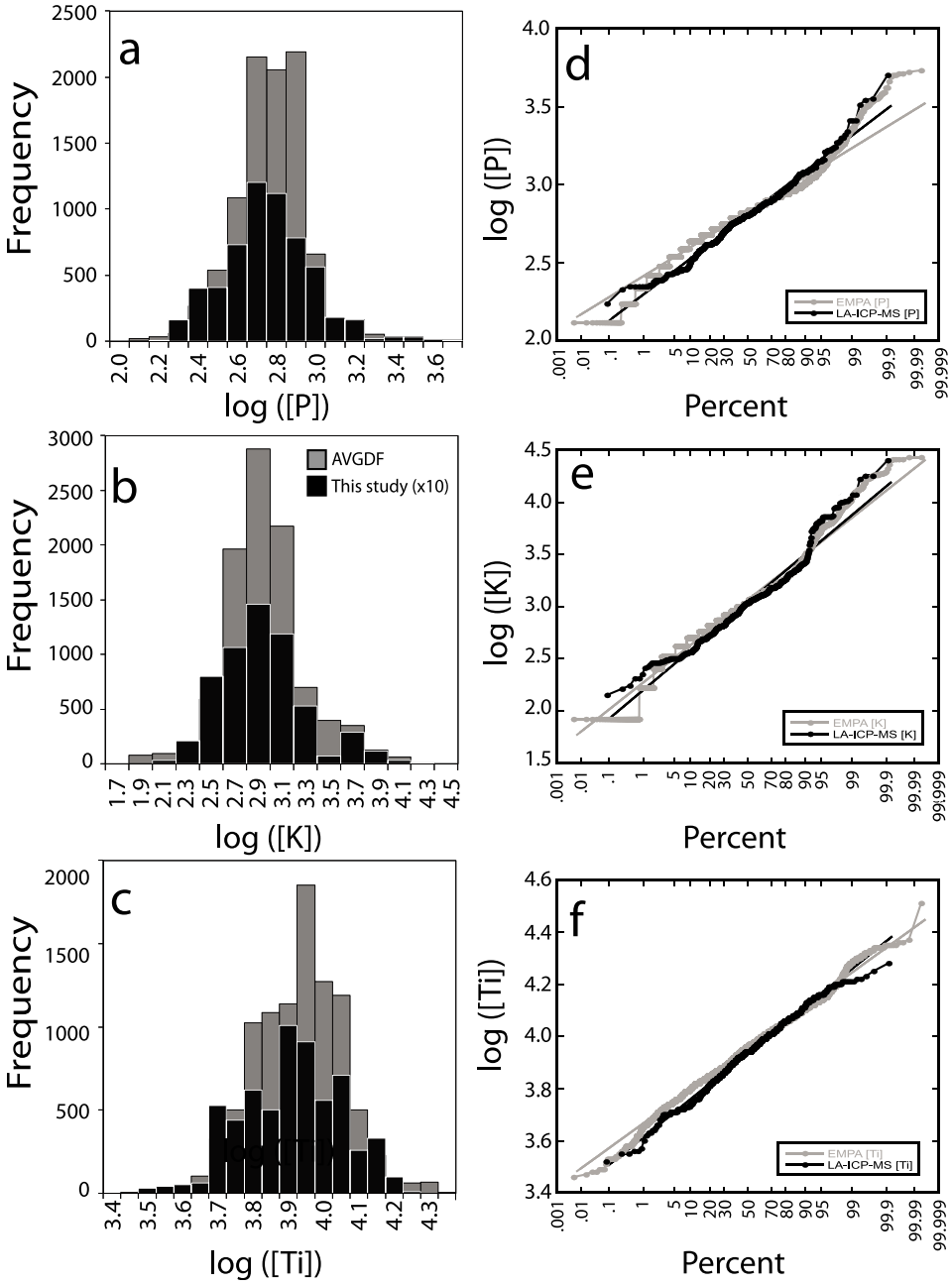

Figure 4. (a–c) Frequency diagrams showing the range in P, K, and Ti contents analyzed here (x10) compared to the range in samples in the AVGDF. (d–f) Cumulative probability (logarithmic scales) for P, K, and Ti. In particular, Ti shows an almost perfect log normal distribution in both the entire AVGDF and the samples analyzed here.

these elements were determined by EMPA. Notably, K, P and Ti, which are representative of the behavior of incompatible trace elements in general, display lognormal distributions with little skewness or kurtosis, in which the number of 'enriched' samples is balanced by an equal tail of 'depleted' samples (Figure 4). The distributions demonstrate a continuum in OFB compositions, supporting previous conclusions [e.g., *Hofmann*, 2003] that there is no fundamental distinction between N-MORB, E-MORB, P-MORB and D-MORB (for Normal-, Enriched-, Plume-, and Depleted-MORB). Making such distinctions is misleading if it is taken to imply discontinuities in the global trace element distributions or the process that produces OFB.

[10] The analyzed samples are from a range of tectonic settings classified in the AVGDF as

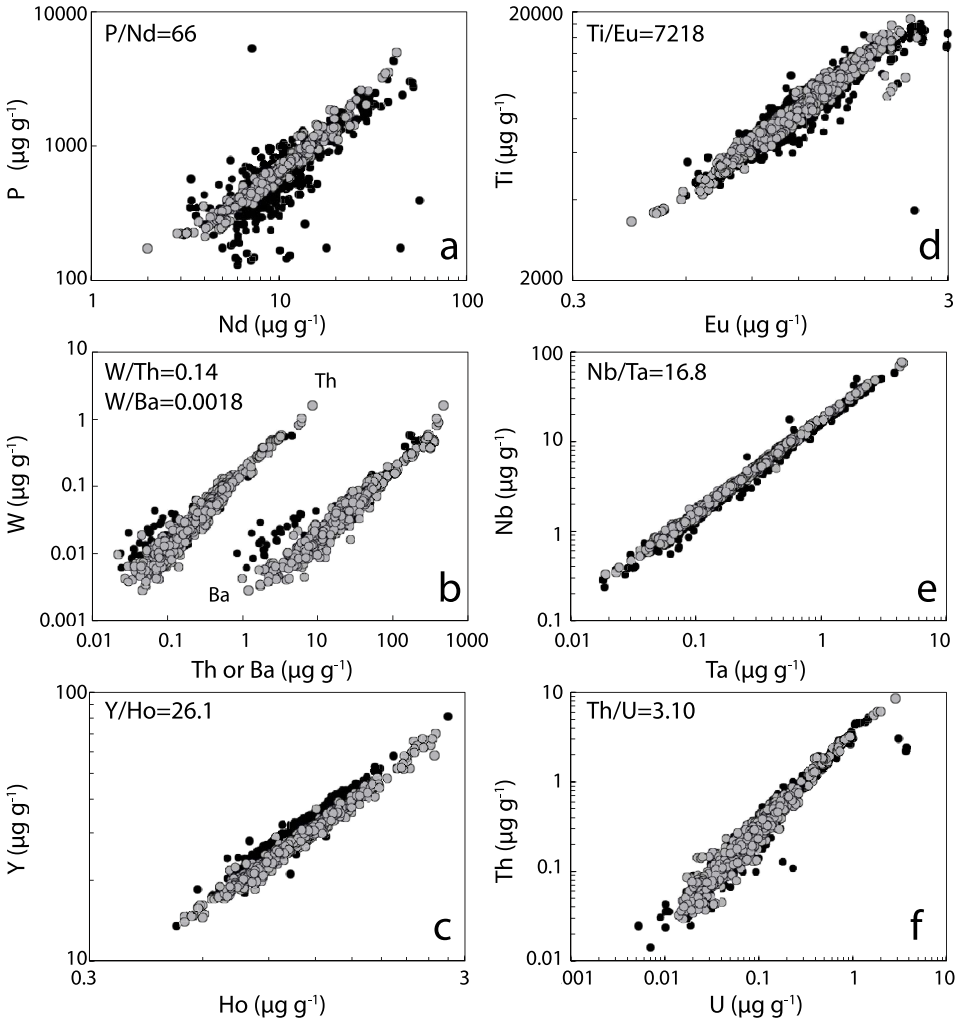

Figure 5. Examples of trace element ratios typically used to interpret basalt petrogenesis, presented here as a demonstration of data quality. Gray symbols are data from this contribution. Black symbols are data analyzed and compiled in the study by *Arevalo and McDonough* [2010]. Values for elemental ratios are calculated by regressing the analyses of one element against another, with weighting of both variables.

spreading ridges (497), seamounts (n = 37), fracture zones (n = 71), aseismic ridges (n = 4) and backarc basins (n = 7). Some of the tectonic settings assigned in the AVGDF are misleading. A number of samples classified as 'spreading centers' are ridges associated with hot spot tracks (Figure 2), such as the Chagos-Laccadive Ridge, considered part of the Réunion hot spot track [e.g., *Fisk et al.*, 1989] and the Cocos Ridge, considered part of the Galapagos hot spot track [e.g., *O'Connor et al.*, 2007]. It is important for interpretation of the global database that these types of tectonic settings are recognized as distinct from the ridges associated with usual seafloor spreading. For example, samples from 11 localities (Figure 2) have higher Cu contents at a given MgO compared to the typical OFB array (Figure 3) Most of these localities have previously been linked to plume-related magmatism, such as the locations mentioned above and the Reykjanes Ridge, south of the Iceland plume [e.g., *Peate et al.*, 2001].

3.2. Trace Element Distributions of the OFB Data File

[11] The application of our results to OFB petrogenesis and the implications for the origin and evolution of the OFB source mantle will be addressed in future contributions. Here we highlight some of the features of the trace element chemistry of OFB glasses as indicators of data quality. Figures 5, 6 and 7 show a selection of

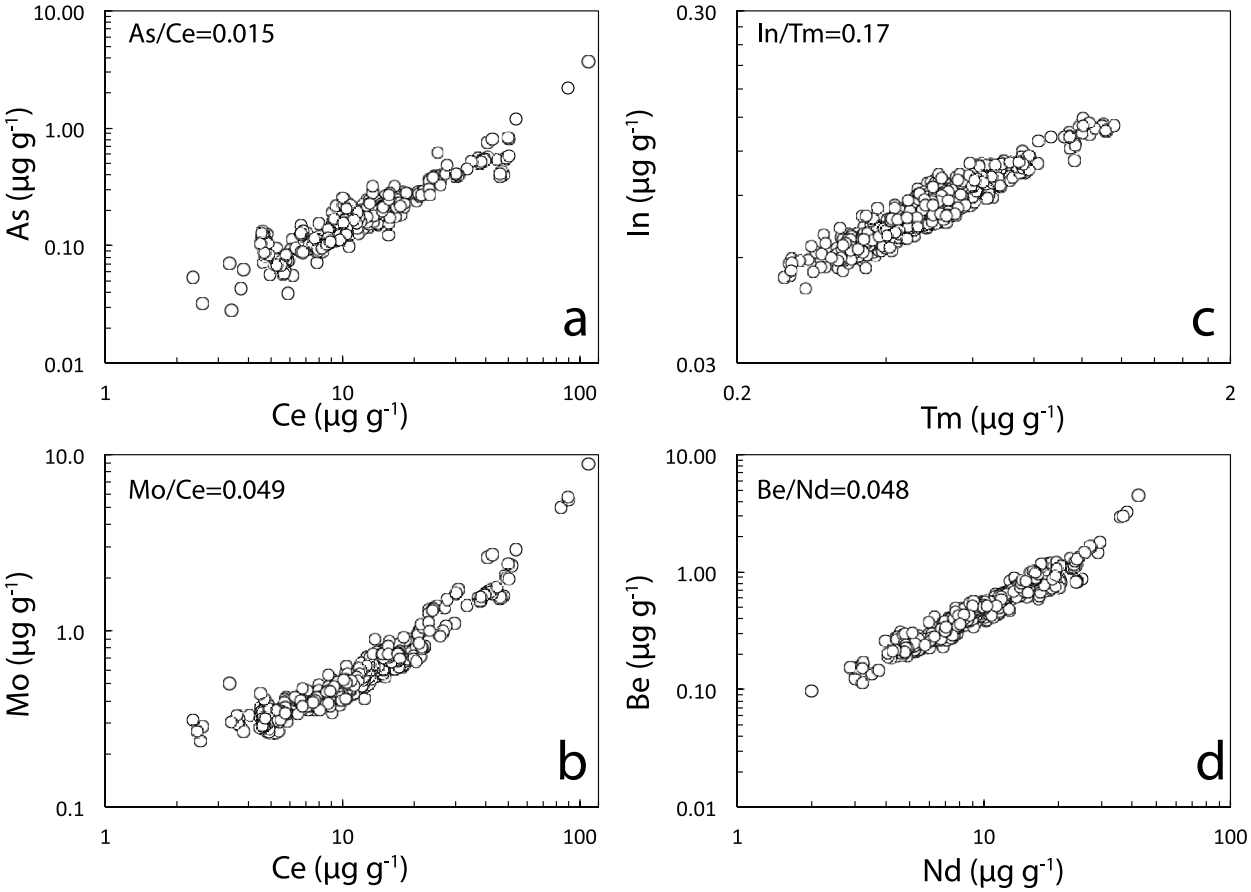

Figure 6. Examples of trace element ratios typically used to interpret basalt petrogenesis, presented here as a demonstration of data quality. Values for elemental ratios are calculated by regressing the analyses of one element against another, with weighting of both variables.

element ratios exploited by geochemists for interpretation of OFB petrogenesis and estimation of the composition of both the primitive and depleted mantle [e.g., *Arevalo and McDonough*, 2010; *Hofmann*, 2003; *Palme and O'Neill*, 2003; *Salters and Stracke*, 2004, and references therein]. The fits to the correlations presented are consistent with uncertainties in the contents of these elements of ±5%, plus the limit of detection, significant here for Cs and U [see *Jenner and O'Neill*, 2012]. Some geochemical trends that emerge from our data imply rather better precision. For example, the deviations from the correlation between Zr and Hf shown in Figure 7 are not random, as Zr/Hf correlates with Nd. Observing this correlation implies that the Zr/Hf can be measured with a precision of 3% and lends support to previous assessments that the Zr/Hf is fractionated by clinopyroxene during low-pressure evolution in crustal magma chambers [e.g., *David et al.*, 2000]. The correlation between Zr/Hf and incompatible element enrichment (as represented here by Nd) extends to Zr/Hf both above and below the chondritic value and holds for samples from each tectonic setting (Figure 7a) and from each ocean basin sampled (Figure 7b).

[12] The data presented here are overall in good agreement with those of *Arevalo and McDonough* [2010], as demonstrated in Figures 5 and 7, but often show less scatter, especially for P/Nd, Zr/Hf, W/Th and W/Ba, indicating an improvement in analytical precision. There is a remarkable uniformity in the trace element geochemistry of OFB for certain ratios of elements with quite different chemical properties, such as that between Nd (a 3+ cation) and either P (5+) or Be (2+) (Figure 5a and 6d, respectively). These ratios are almost constant within analytical uncertainty, with the possible exception of the most evolved samples (<5 wt.% MgO). Especially significant is the improvements to the precision in P/Nd measurements (Figure 5a): the differences in partitioning behavior of these two elements in mantle phases is well documented, with P standing out as the only highly incompatible trace

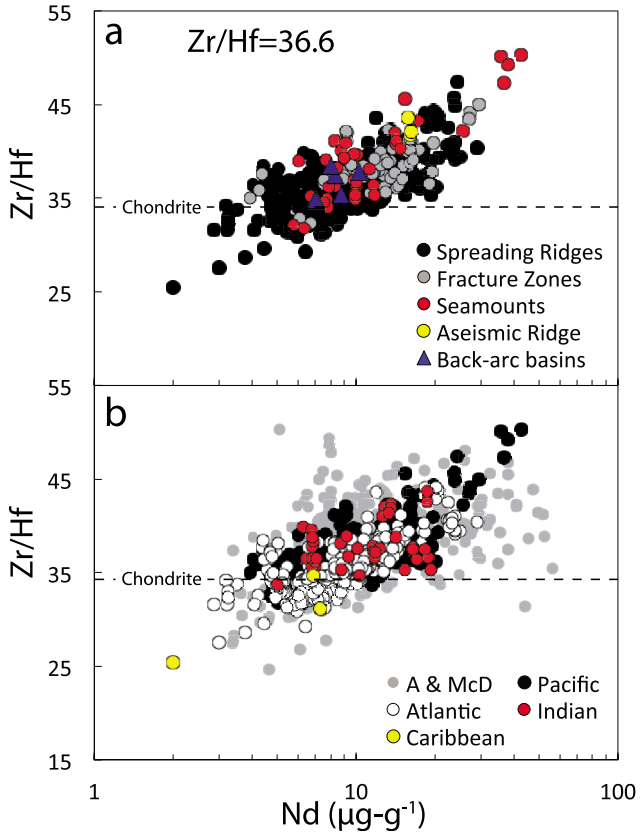

Figure 7. Zr/Hf versus Nd for (a) different tectonic settings and (b) different ocean basins. Zr/Hf in chondrite from *Patzer et al.* [2010]. See text for discussion.

element with affinity for olivine greater than for clinopyroxene [*Mallmann and O'Neill*, 2007, 2009]. The constant P/Nd spanning the entire range of OFB enrichment/depletion does not accord with a role for pyroxenite in the source during partial melting [*O'Neill and Mallmann*, 2007].

[13] The precision of the REE data may be illustrated by the behavior of Eu. Of the REE, Eu behaves anomalously because of its tendency to occur as Eu^{2+} as well as Eu^{3+} (Eu^{2+} readily substitutes for Ca in phases where the Ca site has high coordination number such as plagioclase). The Eu anomaly (Eu/Eu*) is defined as observed Eu divided by Eu expected from interpolation between the abundances of other REE. We calculate Eu* from polynomial fits of the other 13 REE against ionic radius and interpolating to the ionic radius of Eu^{3+}, rather than relying on interpolation between Sm and Gd. The Eu anomaly correlates well with Sr/Sr*, shown in Figures 8e and 8f, resulting from plagioclase fractionation. Our results support the findings of *Niu and O'Hara* [2009] that the most primitive OFB carry distinctly positive Eu/Eu* (also shown in Figures 8a and 8b), which implies that the OFB source has been enriched by addition of material with a positive Eu anomaly relative to the REE. This positive Eu/Eu* seems too large to be attributed to a wrong value in NIST SRM 612, because it would require lowering the GeoReM preferred value of 35.6 $\mu g\ g^{-1}$ to 32 $\mu g\ g^{-1}$, i.e., by 10%. Additionally, the Eu content determined in BCR-2 G is within 0.3% of the GeoReM preferred value [*Jenner and O'Neill*, 2012, Table 6], and Eu contents of the MPI-DING glasses [*Jenner and O'Neill*, 2012, Table 7] are also comparable to the literature values of these reference materials [e.g., *Jochum et al.*, 2006]. The positive Eu anomaly is present in samples from each ocean basin (Figures 8a and 8c) and each tectonic setting (Figures 8b and 8d), demonstrating this is a global feature of the source of OFB. The lack of a Eu/Eu* anomaly in the global MORB average presented by *Arevalo and McDonough* [2010] can be attributed to their calculation of this anomaly at an MgO content of 7.84 wt%. Our results show that the decrease of Eu/Eu* with MgO resulting from low

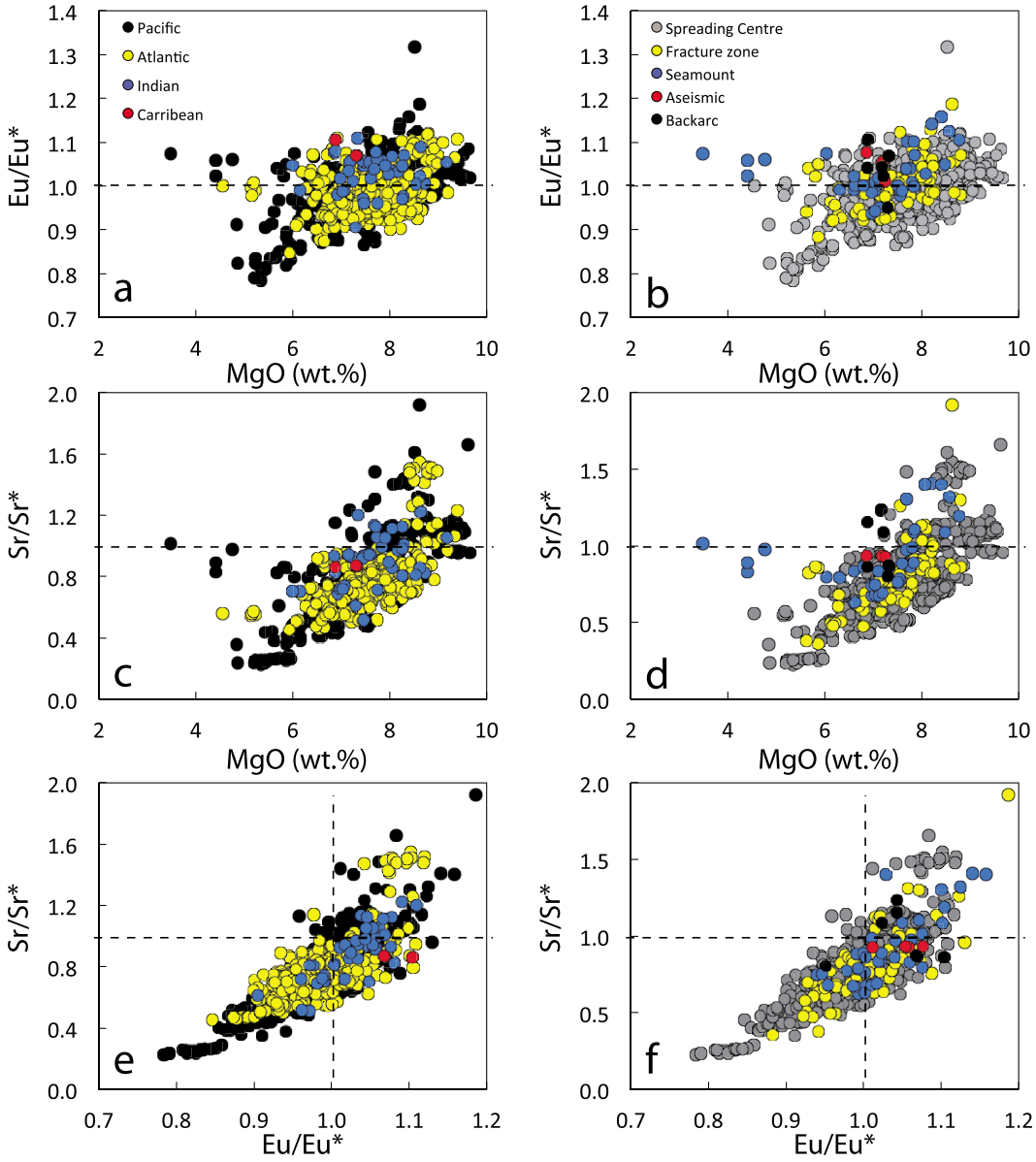

Figure 8. Both (a, b) Eu/Eu* and (c, d) Sr/Sr* decrease with decreasing MgO content, indicative of plagioclase fractionation. Sr/Sr* defined as $2[Sr]_{CI}/([Pr]_{CI} + [Nd]_{CI})$ [*Niu and O'Hara*, 2009]. This trend is observed in samples from each ocean basin (Figures 8a and 8c) and each tectonic setting (Figures 8b and 8d). The systematic nature of the trends are demonstrated by (e, f) the correlation between Eu/Eu* and Sr/Sr*. Notably, the most primitive samples (high MgO) have positive Eu and Sr anomalies (Eu/Eu* and Sr/Sr* > 1), indicating that the mantle source region also has a positive Eu/Eu*.

pressure plagioclase fractionation eliminates the anomaly at this MgO (Figures 8a and 8b).

Acknowledgments

[14] We thank the Smithsonian Institute for the loan of the samples, which made this project possible. Their spirit of generosity in sharing this most valuable resource has been quite exceptional, not to mention inspirational. These samples were in turn donated by many individuals and organizations, funded from many different sources, cutting across national boundaries. The whole enterprise sets the benchmark for how science should be done. We would like to thank Al Hofmann and Andreas Stracke for thorough, constructive and entertaining reviews. Joel Baker is thanked for his editorial skills and review. Richard Arculus and Rick Carlson are thanked for comments and discussion regarding earlier versions of the manuscript.

References

Amante, C., and B. W. Eakins (2009), ETOPO1 1 Arc-Minute Global Relief Model: Procedures, data sources and analysis, *NOAA Tech. Memo. NESDIS NGDC-24*, 25 pp., NOAA, Boulder, Colo. [Available at http://www.ngdc.noaa.gov/mgg/global/global.html.]

Arevalo, R., and W. F. McDonough (2010), Chemical variations and regional diversity observed in MORB, *Chem. Geol.*, *271*, 70–85, doi:10.1016/j.chemgeo.2009.12.013.

Aubaud, C., F. Pineau, A. Jambon, and M. Javoy (2004), Kinetic disequilibrium of C, He, Ar and carbon isotopes during degassing of mid-ocean ridge basalts, *Earth Planet. Sci. Lett.*, *222*(2), 391–406, doi:10.1016/j.epsl.2004.03.001.

Baker, D. R. (2008), The fidelity of melt inclusions as records of melt composition, *Contrib. Mineral. Petrol.*, *156*(3), 377–395, doi:10.1007/s00410-008-0291-3.

Cogné, J. P., and E. Humler (2006), Trends and rhythms in global seafloor generation rate, *Geochem. Geophys. Geosyst.*, *7*, Q03011, doi:10.1029/2005GC001148.

Crisp, J. A. (1984), Rates of magma emplacement and volcanic output, *J. Volcanol. Geotherm. Res.*, *20*(3–4), 177–211, doi:10.1016/0377-0273(84)90039-8.

David, K., P. Schiano, and C. J. Alle (2000), Assessment of the Zr/Hf fractionation in oceanic basalts and continental materials during petrogenetic processes, *Earth Planet. Sci. Lett.*, *178*, 285–301, doi:10.1016/S0012-821X(00)00088-1.

Davis, A. S., D. A. Clague, B. L. Cousens, R. Keaten, and J. B. Paduan (2008), Geochemistry of basalt from the North Gorda segment of the Gorda Ridge: Evolution toward ultraslow spreading ridge lavas due to decreasing magma supply, *Geochem. Geophys. Geosyst.*, *9*, Q04004, doi:10.1029/2007GC001775.

de Hoog, J. C. M., P. R. D. Mason, and M. van Bergen (2001), Sulfur and chalcophile elements in subduction zones: Constraints from a laser ablation ICP-MS study of melt inclusions from Galunggung Volcano, Indonesia, *Geochim. Cosmochim. Acta*, *65*, 3147–3164, doi:10.1016/S0016-7037(01)00634-2.

Fisk, M. R., R. A. Duncan, A. N. Baxter, J. D. Greenough, R. B. Hargraves, and Y. Tatsumi (1989), Reunion hotspot magma chemistry over the past 65 my: Results from Leg 115 of the Ocean Drilling Program, *Geology*, *17*(10), 934–937, doi:10.1130/0091-7613(1989)017<0934:RHMCOT>2.3.CO;2.

Hauri, E., J. Wang, J. E. Dixon, P. L. King, C. W. Mandeville, and S. Newman (2002), SIMS analysis of volatiles in silicate glasses 1. Calibration, matrix effects and comparisons with FTIR, *Chem. Geol.*, *183*, 99–114, doi:10.1016/S0009-2541(01)00375-8.

Hofmann, A. W. (2003), Sampling mantle heterogeneity through oceanic basalts: Isotopes, in *Treatise on Geochemistry*, vol. 2, *The Mantle and Core*, edited by R. W. Carlson, chap. 3, pp. 61–101, Elsevier, Amsterdam.

Hu, Z., Y. Liu, M. Li, S. Gao, and L. Zhao (2009), Results for rarely determined elements in MPI-DING, USGS and NIST glasses using laser ablation ICP-MS, *Geostand. Geoanal. Res.*, *33*, 319–335, doi:10.1111/j.1751-908X.2009.00030.x.

Jarosewich, E., J. A. Nelen, and J. A. Norberg (1979), Electron microprobe reference samples for mineral analyses, *Smithson. Contrib. Earth Sci.*, *22*, 68–72.

Jenner, F. E., H. St. C. O'Neill, R. J. Arculus, and J. A. Mavrogenes (2010), The magnetite crisis in the evolution of arc-related magmas and the initial concentration of Au, Ag, and Cu, *J. Petrol.*, *51*(12), 2445–2464, doi:10.1093/petrology/egq063.

Jenner, F. E., and H. St. C. O'Neill (2012), Major and trace analysis of basaltic glasses by laser-ablation ICP-MS, *Geochem. Geophys. Geosyst.*, doi:10.1029/2011GC003890, in press.

Jochum, K. P., B. Stoll, K. Herwig, M. Willbold, and A. W. Hoffman (2006), MPI-DING reference glasses for insitu microanalysis: New reference values for element concentrations and isotope ratios, *Geochem. Geophys. Geosyst.*, *7*, Q02008, doi:10.1029/2005GC001060.

Kamenetsky, V. S., M. B. Kamenetsky, V. V. Sharygin, K. Faure, and A. V. Golovin (2007), Chloride and carbonate immiscible liquids at the closure of the kimberlite magma evolution (Udachnaya-East kimberlite, Siberia), *Chem. Geol.*, *237*(3–4), 384–400, doi:10.1016/j.chemgeo.2006.07.010.

Keays, R. R. (1987), Principles of mobilization (dissolution) of metals in mafic and ultramafic rocks—The role of immiscible magmatic sulphides in the generation of hydrothermal gold and volcanogenic massive sulphide deposits, *Ore Geol. Rev.*, *2*, 47–63, doi:10.1016/0169-1368(87)90023-0.

Laubier, M., P. Schiano, R. Doucelance, L. Ottolini, and D. Laporte (2007), Olivine-hosted melt inclusions and melting processes beneath the FAMOUS zone (Mid-Atlantic Ridge), *Chem. Geol.*, *240*(1–2), 129–150, doi:10.1016/j.chemgeo.2007.02.002.

Mallmann, G., and H. St. C. O'Neill (2007), The effect of oxygen fugacity on the partitioning of Re between crystals and silicate melt during mantle melting, *Geochim. Cosmochim. Acta*, *71*(11), 2837–2857, doi:10.1016/j.gca.2007.03.028.

Mallmann, G., and H. St. C. O'Neill (2009), The crystal/melt partitioning of V during mantle melting as a function of oxygen fugacity compared with some other elements (Al, P, Ca, Sc, Ti, Cr, Fe, Ga, Y, Zr and Nb), *J. Petrol.*, *50*(9), 1765–1794, doi:10.1093/petrology/egp053.

Mathez, E. A. (1976), Sulfur solubility and magmatic sulphides in submarine basalt glass, *J. Geophys. Res.*, *81*(23), 4269–4276, doi:10.1029/JB081i023p04269.

Melson, W. G., T. Vallier, T. L. Wright, G. Byerly, and J. Nesen (1976), Chemical diversity of abyssal volcanic glass erupted along seafloor spreading centers, in *The Geophysics of the Pacific Ocean Basin and Its Margin*, *Geophys. Monogr. Ser.*, vol. 19, edited by G. H. Sutton et al., pp. 351–367, AGU, Washington, D. C., doi:10.1029/GM019p0351

Melson, W. G., T. O'Hearn, and E. Jarosewich (2002), A data brief on the Smithsonian Abyssal Volcanic Glass Data File, *Geochem. Geophys. Geosyst.*, *3*(4), 1023, doi:10.1029/2001GC000249.

Niu, Y., and J. O'Hara (2009), MORB mantle hosts the missing Eu (Sr, Nb, Ta and Ti) in the continental crust: New perspectives on crustal growth, crust–mantle differentiation and chemical structure of oceanic upper mantle, *Lithos*, *112*(1–2), 1–17, doi:10.1016/j.lithos.2008.12.009.

O'Connor, J. M., P. Stoffers, J. R. Wijbrans, and T. J. Worthington (2007), Migration of widespread long-lived volcanism across the Galápagos Volcanic Province: Evidence for a broad hotspot melting anomaly?, *Earth Planet. Sci. Lett.*, *263*(3–4), 339–354, doi:10.1016/j.epsl.2007.09.007.

O'Neill, H. St. C., and G. Mallmann (2007), The P/Nd ratio of basalt as an indicator of pyroxenite in its source, *Geochim. Cosmochim. Acta*, *71*, suppl. 1, A741.

O'Neill, H. St. C., and J. A. Mavrogenes (2002), The sulfide capacity and the sulfur content at sulfide saturation of silicate melts at 1400 °C and 1 bar, *J. Petrol.*, *43*(6), 1049–1087, doi:10.1093/petrology/43.6.1049.

Palme, H., and H. St. C. O'Neill (2003), Compositional estimates of mantle composition, in *Treatise on Geochemistry*, vol. 2, *The Mantle and Core*, edited by R. W. Carlson, chap. 1, pp. 1–38, Elsevier, Amsterdam.

Paonita, A., and M. Martelli (2007), A new view of the He-Ar-CO_2 degassing at mid-ocean ridges: Homogeneous composition of magmas from the upper mantle, *Geochim. Cosmochim. Acta*, *71*, 1747–1763, doi:10.1016/j.gca.2006.12.019.

Patzer, A., A. Pack, and A. Gerdes (2010), Zirconium and hafnium in meteorites, *Meteorit. Planet. Sci.*, *45*(7), 1136–1151, doi:10.1111/j.1945-5100.2010.01076.x.

Peach, C. L., E. A. Mathez, and R. R. Keays (1990), Sulfide melt-silicate melt distribution coefficients for noble metals and other chalcophile elements as deduced from MORB: Implications for partial melting, *Geochim. Cosmochim. Acta*, *54*(12), 3379–3389, doi:10.1016/0016-7037(90)90292-S.

Peate, D. W., C. J. Hawkesworth, P. W. van Calsteren, R. N. Taylor, and B. J. Murton (2001), ^{238}U–^{230}Th constraints on mantle upwelling and plume–ridge interaction along the Reykjanes Ridge, *Earth Planet. Sci. Lett.*, *187*(3–4), 259–272, doi:10.1016/S0012-821X(01)00266-7.

Ryan, W. B. F., et al. (2009), Global Multi-Resolution Topography synthesis, *Geochem. Geophys. Geosyst.*, *10*, Q03014, doi:10.1029/2008GC002332.

Salters, V. J. M., and A. Stracke (2004), Composition of the depleted mantle, *Geochem. Geophys. Geosyst.*, *5*, Q05B07, doi:10.1029/2003GC000597.